Solar Energy Materials & Solar Cells 251 (2023) 112156

Contents lists available at ScienceDirect

Solar Energy Materials and Solar Cells

journal homepage: www.elsevier.com/locate/solmat

Hole selective contacts based on transition metal oxides for c-Ge thermophotovoltaic devices

Isidro Martín [a,*], Gema López [a], Moisés Garín [b], Eloi Ros [a], Pablo Ortega [a], Cristóbal Voz [a], Joaquim Puigdollers [a]

[a] Departament d'Enginyeria Electrònica, Universitat Politècnica de Catalunya, Jordi Girona 1-3, Barcelona, 08034, Spain
[b] GR-MECAMAT, Department of Engineering, Universitat de Vic – Universitat Central de Catalunya, c/de la Laura 13, 08500, Vic, Spain

ARTICLE INFO

Keywords:
Termophotovoltaics
Germanium
Selective contacts

ABSTRACT

Thermophotovoltaics has become a very attractive solution for heat-to-electricity conversion due to its excellent conversion efficiencies. However, further research is needed to reduce the device cost which is typically based on III-V semiconductors. To tackle this limitation, crystalline germanium (c-Ge) has been proposed as an excellent substrate for low-cost devices. One of the key advances behind high system efficiencies is the excellent reflectance of the out-of-band photons at the rear surface of the photovoltaic device. These photons with lower energy than the absorber bandgap are reflected back to the thermal emitter reducing its thermal losses. In this work, we explore the performance of hole selective contacts based on evaporated transition metal oxides (MoO_x, VO_x, WO_x) to be introduced at the rear surface of c-Ge devices. Regarding electrical properties, we characterize the selectivity of the contact by measuring effective surface recombination velocity (S_{eff}) and contact resistivity (ρ_C). Best results are obtained with MoO_x contacted by Ag/ITO with $S_{eff} = 588$ cm/s and $\rho_C = 55.6$ mΩ cm^2 which can be improved by using gold as a metal contact leading to $S_{eff} = 156$ cm/s and $\rho_C = 60.9$ mΩ cm^2. Regarding out-of-band reflectance, it is better for the case of Ag/ITO/MoO_x contact with 87.5% compared to 78.9% for Au/MoO_x when a 1473 K black body spectrum is used. Device simulations show potential system efficiencies in the range of 18–19% which are comparable to the best reported efficiencies using c-Ge thermophotovoltaic devices.

1. Introduction

Thermophotovoltaics (TPV) is based on the heat-to-electricity conversion using a photovoltaic cell which exploits the infrared photons emitted by a hot body [1]. These systems have the potential to achieve very high efficiencies and power densities due to the absence of movable parts and the proximity of the hot thermal emitter. As a consequence, they have become a promising approach to different energy applications like space power [2], energy storage [3,4], waste heat recovery [5] and solar energy conversion [6,7]. However, further technological development is needed to reduce the cost per watt of TPV systems to make it competitive in front of other renewal energy sources. To do so, one of the approaches is to improve system conversion efficiencies where values in the range of 30% [8–10] and even up to 40% [11] have been recently reported. One of the key advances behind these high efficiencies is an excellent reflectance of the out-of-band photons, i.e. photons whose energy is lower than the bandgap of the absorber, at the rear surface of the photovoltaic device. By doing so, these photons are reflected back to the thermal emitter reducing its thermal losses and improving system efficiency. For further reduction of the device cost, crystalline germanium (c-Ge) has been proposed as an excellent substrate for TPV low-cost devices [12,13] in front to the III-V semiconductors used as the low bandgap absorbers [8–11].

In this work, we combine the two strategies mentioned above by exploring the potential of transition metal oxides (TMO's) as hole selective contacts at the rear surface of p-type c-Ge TPV devices. In particular, we use molybdenum oxide (MoO_x), vanadium oxide (VO_x) and tungsten oxide (WO_x), which have been successfully used as hole selective contacts on silicon [14–17]. Regarding c-Ge substrates, MoO_x has been reported as hole selective contact on n-type substrates being responsible for creating the junction [18], but no previous work has been published using TMO's as majority carrier contacts, i.e. using p-type c-Ge wafers. Due to its novelty, the main objective of this work is to demonstrate the suitability of this approach leaving further contact

* Corresponding author.
E-mail address: isidro.martin@upc.edu (I. Martín).

https://doi.org/10.1016/j.solmat.2022.112156
Received 20 October 2022; Received in revised form 12 December 2022; Accepted 13 December 2022
Available online 21 December 2022

optimization, like layer thickness or the incorporation of the contact to finished devices, for future research.

2. Experimental

As substrates, we used double side polished 175 μm thick (100) p-type c-Ge wafers with resistivity 1.2 Ω cm which corresponds to an acceptor doping density of $2.1{\cdot}10^{15}$ cm^{-3}. To clean the germanium surface and remove native oxide, we used a HCl:H_2O (1:1) dip for 3 min. In case that the TMO layer was deposited directly onto germanium surface, samples were immediately loaded into a thermal evaporator tool to deposit ~20 nm-thick layers of MoO_x, VO_x and WO_x. In order to improve surface passivation, in some cases we introduced a thin (~2 nm) layer of silicon rich amorphous silicon carbide (a-SiC_x) deposited by Plasma Enhanced Chemical Vapor Deposition. This layer has demonstrated a significant reduction of the interface state density [19] and it is kept thin to reduce its impact on carrier transport. In order to contact the TMO layers, we used Indium Tin Oxide (ITO) which was deposited by sputtering capped with a layer of evaporated silver. Alternatively, we also used thermally evaporated gold directly on the TMO material.

To evaluate electrical properties of the contacts, we measured the effective surface recombination velocity (S_{eff}) and the contact resistivity (ρ_C). For the S_{eff} measurement, we applied Quasi-Steady State Photoconductance technique [20] using commercial tool Sinton WCT-120 where a flash lamp is photogenerating carriers and their evolution in time is recorded by measuring the photoconductivity of the sample through inductive coupling. This tool is widely applied to determine surface recombination in crystalline silicon and, recently, its applicability to crystalline germanium has been demonstrated as well [21]. Using this measurement, the dependence of the effective lifetime (τ_{eff}) on the excess carrier density (Δn) is obtained. Integrating all the recombination mechanisms in the sample we obtain:

$$\frac{1}{\tau_{eff}} = \frac{1}{\tau_b} + \frac{S_{eff|front}}{w} + \frac{S_{eff|rear}}{w} \tag{1}$$

where τ_b is the bulk recombination lifetime, w is the thickness of the wafer and $S_{eff|front}$ ($S_{eff|rear}$) is the effective surface recombination at the front (rear) surface.

Examples of the measured $\tau_{eff}(\Delta n)$ curves is shown in Fig. 1. In particular, we show the measurement of a c-Ge substrate symmetrically covered with 22 nm thick amorphous silicon carbide layers (a-SiC_x). In this case, assuming negligible bulk recombination, i. e τ_b tending to infinity, and equal S_{eff} value at both surfaces, we can calculate an upper bound of the S_{eff}. For this calculation and any other S_{eff} value reported in this paper, we use the τ_{eff} value at $\Delta n = 5{\cdot}10^{14}$ cm^{-3} (indicated by the red arrow in the graph). For this symmetrical sample, τ_{eff} is equal to 520 μs leading to a S_{eff} of 17 cm/s. This value is also used for the determination of the S_{eff} values related to the TMOs. In the fabricated samples, whose cross-section can be also seen in Fig. 1, we deposited the amorphous silicon carbide layer at the rear surface while on front surface we define the corresponding hole selective contact under exploration. As a result, we obtained $\tau_{eff}(\Delta n)$ curves like the one shown in Fig. 1 and the S_{eff} at the selective contact surface can be calculated using equation (1) with τ_b tending to infinity and $S_{eff|rear} = 17$ cm/s. In the example shown in Fig. 1, a S_{eff} of 588 cm/s for the hole selective contact is calculated.

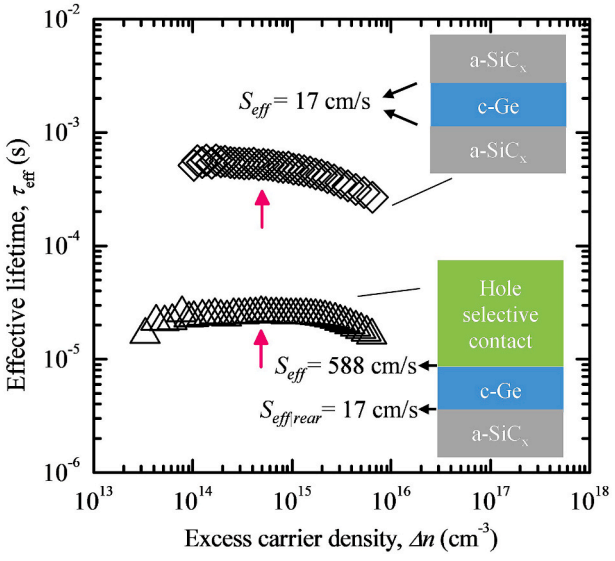

Fig. 1. Examples of the $\tau_{eff}(\Delta n)$ curves measured using Sinton WCT-120. The corresponding S_{eff} is calculated using equation (1) with τ_{eff} value at $\Delta n = 5{\cdot}10^{14}$ cm^{-3} which is indicated by the arrow.

Regarding contact resistivity, we applied Transfer Length Method [22]. In this technique, contacts are defined with different distances and the resistance between them is measured. In our case, we define 1 cm × 200 μm contact pads separated 250, 350, 450 and 550 μm. The resistance linearly increases with the distance between contacts due to the current flowing through a longer piece of wafer. As a consequence, applying a linear fit, we can extrapolate this dependence to the point without distance between contacts, i.e. the y-axis crossing point where only contact resistance is considered. In particular, the obtained value is two times the contact resistance which is then transferred to contact resistivity (ρ_C) by applying the geometry of the contact pads following equation (3) in Ref. [22] (see Supplementary Information file for further details). In Fig. 3, we show an example of the measured data using this method together with the typical cross-section of the samples.

Finally, good selective contacts must simultaneously have low S_{eff} and ρ_C. In order to summarize the electrical quality of the contact, Brendel and Peibst proposed the contact selectivity parameter (S_{10}) defined as [23]:

$$S_{10} = \log_{10}\left(\frac{v_{th}}{J_0{\cdot}\rho_C}\right) \tag{2}$$

where v_{th} is the thermal voltage and J_0 is the saturation current density which is an alternative way to quantify surface recombination. In particular, J_0 can be calculated from S_{eff} applying:

$$S_{eff} = \frac{J_o}{q}\frac{(N_{dop} + \Delta n)}{{n_i}^2} \tag{3}$$

Where q is the fundamental charge, n_i is the excess carrier density of the semiconductor and N_{dop} is the bulk doping density. In our case, we use $n_i = 2.33{\cdot}10^{13}$ cm^{-3}, a doping density of $2.1{\cdot}10^{15}$ cm^{-3} and $\Delta n = 5{\cdot}10^{14}$ cm^{-3} where we calculate the corresponding S_{eff}. We will use the S_{10} parameter as a figure of merit to evaluate the different explored contacts in this work.

3. Results and discussion

3.1. Electrical performance of TMOs contacted by ITO

Following the experimental procedure described in the previous section, we evaluate the S_{eff} provided by the three explored transition metal oxides namely VO_x, MoO_x, WO_x contacted by 80 nm of ITO. In this case, the evaporated silver was not evaporated on top because the passivating properties do not change with it since the contact is already created. The results are shown in Fig. 2. As we can see, S_{eff} values of 588 and 712 cm/s are obtained in the as deposited state for MoO_x and VO_x samples respectively, while a much worse result with S_{eff} beyond 3500 cm/s is measured for the WO_x. In order to improve surface passivation, a thin (~2 nm) a-SiC_x layer was introduced between the TMO and the c-Ge substrate. As can be seen in Fig. 2, the introduction of this layer leads to a much better result with S_{eff} of about 300 cm/s for all three TMOs which

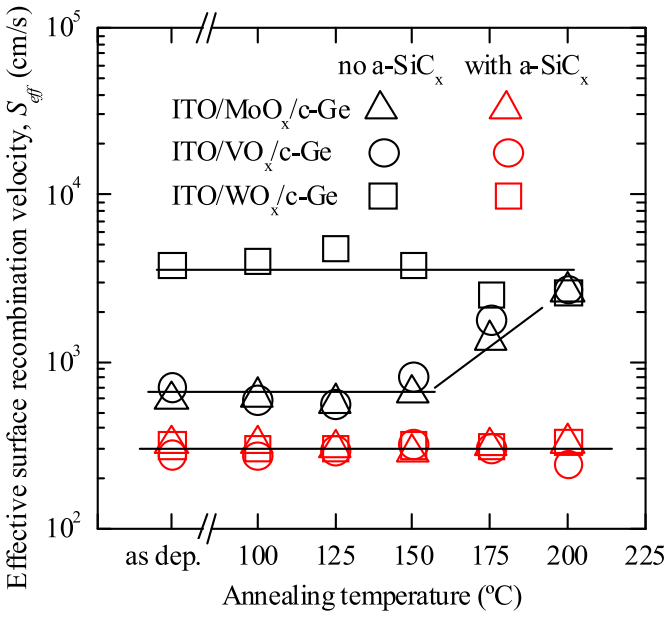

Fig. 2. S_{eff} values measured for the TMO contacts contacted by ITO with and without a thin (~2 nm) a-SiC$_x$ interlayer. The introduction of such layer results in better passivation most likely due to a reduction of the interface state density. Additionally, stability with annealing is also improved with constant values up to 200 °C. Lines are a guide to the eye.

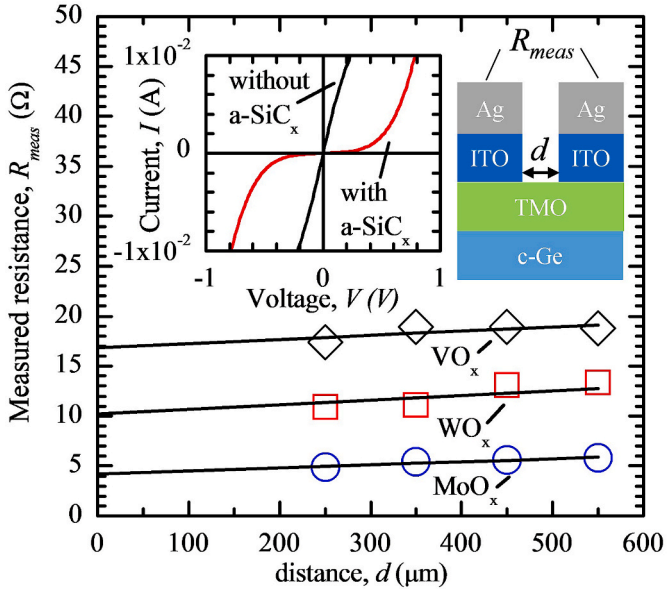

Fig. 3. Measured resistance as a function of the distance between contacts leading to linear trends which permit to calculate contact resistivity by applying the Transfer Length Method (TLM). Contact resistivity is calculated from the y-axis cross point and applying the contact area. (inset) I–V curves of the MoO$_x$ with and without a-SiC$_x$ interlayer. A rectifying behaviour is found when this thin film is introduced.

can be interpreted as a reduction of the interface state density, as reported in Ref. [19]. Importantly, we have also characterized the thermal stability of the passivation with cumulative annealings in Forming gas (N_2/H_2, 95/5%) of 10 min. We can see how the surface passivation provided for ITO/MoO$_x$ and ITO/VO$_x$ directly deposited on the c-Ge surface is stable up to 150 °C and then passivation degrades. In the case of introducing the thin (~2 nm) a-SiC$_x$ film passivation is stable in the explored range up to 200 °C. This improvement indicates that the degradation mechanism is impacted by the presence of an amorphous silicon rich film between TMO and c-Ge substrate, similarly to the reported results in c-Si substrates [24]. It must be mentioned that, apart from the inherent value of the information, thermal stability can be relevant more in the compatibility of this contact with the rest of the device fabrication process than in device performance because thermophotovoltaic devices are typically maintained to about room temperature to provide reasonable efficiencies (see for example references [8,9] where a water cooling system is used).

Once the surface passivation quality has been determined, we prepared samples for measuring the contact resistivity by the TLM method where the ITO is contacted by 1 μm of evaporated silver to keep the contact under equipotential conditions (see Fig. 3 where a cross-section of the sample is shown). Deviations from this conditions are taken into account by measuring the resistance of the finger and subtracting it from the measured resistance following reference [22]. For all the samples with the thin a-SiC$_x$ layer we measure non-linear current-voltage (I–V) curves while the absence of this layer leads to ohmic contacts. To illustrate this point, we show in the inset of Fig. 3 the I–V curves measured for the MoO$_x$ sample, but similar curves are obtained for the other TMOs. This result indicates that the introduction of the a-SiC$_x$ layer jeopardizes carrier transport through the interface leading to a rectifying contact while the contact becomes ohmic without this layer. As a consequence, only reliable values for the resistance are obtained for the samples without a-SiC$_x$. We apply the TLM method to these samples leading to experimental curves shown in Fig. 3 where the measured resistance (R_{meas}) as a function of the distance (d) between contacts is plotted. As we can see, a linear trend is found for all three samples with similar slope which is related to the sheet resistance of the c-Ge substrate. As it was mentioned in the experimental section, the contact resistivity is calculated from the y-axis crossing point of the linear trends and the best result, i.e. the lowest value of the contact resistivity, corresponds to the MoO$_x$ material. The obtained ρ_C values together with the corresponding S_{eff} ones are summarized in Table 1. Additionally, the effective surface recombination is translated to saturation current density (J_0), also shown in the table, using equation (3) which enables the calculation of the contact selectivity parameter (S_{10}) through equation (2). As can be seen in Table 1, the highest S_{10} value corresponds to the Ag/ITO/MoO$_x$ sample mainly because of the low ρ_C value. For VO$_x$ similar passivation is found, but with worse carrier transport properties, while WO$_x$ has very poor surface passivation.

3.2. Electrical performance of MoO$_x$ contacted by gold

Based on the above results, we focused on the MoO$_x$ as the most promising material for a hole selective contact for c-Ge devices. In order to improve its performance, we investigate the selectivity of the contact when it is contacted by thermally evaporated gold instead of ITO. In previous experiments, a degradation of the surface passivation quality was identified during the sputtering process of the ITO deposition which can be avoided if thermal evaporation is used. In addition, a gold contact on MoO$_x$ was already reported in the literature for crystalline silicon devices [16]. Finally, gold is used in high efficiency TPV systems as the rear contact of the device due to its high reflectance for the out-of-band photons [8,9].

Table 1
S_{eff} and ρ_C experimental values for the explored hole selective contacts. The calculated J_0 and S_{10} values are also shown.

	ρ_C (mΩ·cm^2)	S_{eff} (cm/s)	J_0 (μA/cm^2)	S_{10}
Ag/ITO/MoO$_x$	55.6	588	19.6	4.4
Ag/ITO/VO$_x$	245.7	712	23.8	3.6
Ag/ITO/WO$_x$	146.2	3787	126.5	3.1
Au/MoO$_x$	60.9	156	5.1	4.9
Au/MoOx/a-SiC$_x$	104.0	139	4.6	4.7

We repeated the procedure to determine S_{eff} using Au as a contact for two samples: with and without the thin a-SiC_x interlayer. In contrast to the previous experiment where silver was not considered in the passivating samples, now the gold layer is impacting on the contact creation, so it is needed for a correct characterization of passivating properties. In this case, a thin (~10 nm) gold layer was used to prevent saturation of the amplifier of the Sinton WCT-120 instrument due to the high gold conductivity, while the effect of metal layer on surface configuration is maintained. The obtained S_{eff} results are shown in Table 1 where we can see that S_{eff} is reduced well below 200 cm/s for both cases which can be linked to the gentler deposition technique of the contact. As in the previous section, the best passivation (S_{eff} = 139 cm/s) is obtained with the a-SiC_x layer, most likely due to the reduction of interface state density.

Regarding contact resistivity, we apply TLM method leading to ohmic contacts on both samples. This result is surprising taking into account that a rectifying behaviour was observed for the sample with a-SiC_x and contacted by ITO (see inset Fig. 3). As reported in Ref. [18], carrier transport at the MoO_x/c-Ge contact consists of electrons from the conduction band of the MoO_x being injected by tunneling through MoO_x gap states close to the interface into the valence band of the c-Ge. This transport mechanism is similar to the one reported in silicon (see for example reference [25] and references therein) and it depends on the hole concentration at the c-Ge surface and the presence of transport barriers to charge carriers. Keeping this in mind, we can see the a-SiC_x layer as a transport barrier that is easier to overcome when gold is used as the metal contact, i.e. gold creates a higher hole density at the c-Ge surface compared to ITO. We think that increase in hole density could be related to the relatively high workfunction of the gold (~5.2 eV) compared to ITO (the most common values for ITO workfunction are in the range of 4.4–4.8 eV [26–29]) which places the Fermi level of the contacting material well below its position in the c-Ge substrate (substrate workfunction is about 4.6 eV). As a consequence, when the selective contact is created a stronger electric field at the interface might be induced increasing the hole density at the c-Ge surface and helping them to be transported through the deposited material stack. Notice that despite creating an ohmic contact, the presence of the a-SiC_x film still increases the contact resistivity to 104.0 mΩ cm^2 compared to its counterpart without this layer (60.9 mΩ cm^2) which indicates the presence of a transport barrier. Despite the mechanism described hereby is a reasonable interpretation of the results, a deeper knowledge of the band structure and interface characteristics of MoO_x/c-Ge is needed to fully understand how carrier transport mechanism takes place.

Finally, the obtained ρ_C values together with the corresponding S_{eff} when gold is used are combined to calculate the corresponding S_{10} parameter (all shown in Table 1) which improves up to 4.9 for the sample without a-SiC_x. In this case, the better surface passivation provided by the a-SiC_x interlayer is compensated by the increase in contact resistivity resulting in a worse contact selectivity.

3.3. Internal optical reflectance of out of band photons

As we have seen in the previous section, selective contacts based on MoO_x are the ones with the best electrical performance for both ITO or gold contacts. Focusing on these two selective contacts, we characterized the optical reflectance of the photons whose energy is lower than the bandgap, i.e. out-of-band photons. These photons are not contributing to the photovoltaic performance and they should be internally reflected at the rear surface of the device and returned back to the thermal emitter to reduce its thermal losses. We carried out reflectance measurements at quasi-normal incidence (13°) using a FT-IR Bruker Vertex 70. In this case, the contact to characterize was defined at the rear surface while the front surface was kept bare. A cross-section of the samples used can be seen in the inset of Fig. 4. These measurements were carried out in a photon energy range from 0.2 to 0.7 eV (1.77–6.20 μm in wavelength) and with a resolution of 8 cm^{-1} to average optical interferences in the bulk.

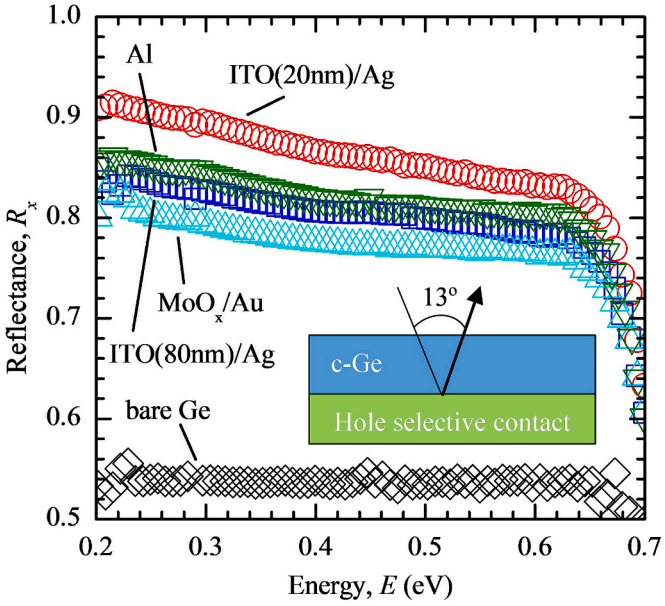

Fig. 4. Experimental reflectance of the hole selective contacts based on MoO_x deposited at the rear surface of c-Ge wafer. A sample of bare c-Ge and with rear surface covered by aluminum are also shown for a direct comparison. Better external reflectance is observed for the case of ITO contact compared to gold which is improved when ITO thickness is reduced to 20 nm. (For interpretation of the references to colour in this figure legend, the reader is referred to the Web version of this article.)

As can be seen in Fig. 4, the results show an increase of the reflectance for both contacts up to about 80–85% compared to the case of bare c-Ge (~55%), which is also included in the plot. As a reference of rear reflecting contact, we also measured the reflectance of a sample with an aluminum film directly deposited on the rear c-Ge surface. As we can see, reflectance is very similar to the ones obtained for the MoO_x contacts indicating a similar performance. Among the explored contacts, the one with ITO shows a slightly higher internal reflectance compared to gold which can be further improved if the thickness of the ITO is reduced to 20 nm leading to values beyond 90% for the lowest energy part of the spectrum. This improvement suggests that free carrier absorption in the ITO is limiting the internal reflectance performance of such contacts.

These results are promising taking into account that no further optimization of the contact structure has been done which is not a straightforward process. For example, all these results are measured using a 175 μm thick c-Ge substrate which provides a significant free carrier absorption. In fact, this effect is enhanced when the device is operating under thermophotovoltaic conditions where the thermal emitter is close to its surface creating a high excess carrier density due to a strong photogeneration rate. This is one of the reasons why the best reflectance results reported in the literature for III-V semiconductor use absorber thicknesses in the range of a few microns [8,9]. Due to the optical absorption coefficients of the c-Ge, a few tens of microns of this material can be enough to absorb a significant percentage of the incoming photons, despite some reduction of the output power is unavoidable. As a consequence, a trade off between photovoltaic performance and reflectance of out-of-band photons exists as a function of the absorber thickness. Moreover, substrate thickness also impacts the optimization of film thicknesses at the rear surface from an optical point of view. As a consequence, all this procedure is beyond the scope of this paper and it will be published elsewhere.

3.4. Simulations of potential system efficiencies

Finally, we perform simulations of potential system efficiencies for thermophotovoltaic devices whose rear contact incorporates the two best MoO_x contacts, i.e. Ag/ITO (20 nm)/MoO_x and Au/MoO_x. In this case, we use the ITO of 20 nm because it does not significantly change the electrical performance of the contact, but it improves its optical response. As a figure of merit, we define the Power Conversion Efficiency (PCE) as:

$$PCE = \frac{P_{electrical}}{P_{incident} - P_{reflected}} \quad (4)$$

Where $P_{incident}$ is the incident power where we consider a black body at 1473 K with a view factor of 0.15, similar to the one reported in Ref. [9], which leads to an incident power of 3.9 W/cm^2; $P_{reflected}$ is the power reflected back to the thermal emitter which is calculated using the experimental reflectance values multiplied by the incident spectrum (S_{1473K} (E)) and integrating the results for the out-of-band photons (a bandgap of 0.67 eV is considered for the c-Ge):

$$P_{reflected} = \int_{0.2}^{E_{GAP}} R_x(E) \cdot S_{1473K}(E) \cdot dE \quad (5)$$

Finally, the electrical power extracted from the photovoltaic device ($P_{electrical}$) is calculated using device simulator PC-1D [29] where we defined a 175 μm thick 1.2 Ω cm p-type germanium absorber where only intrinsic recombination is considered, i.e. Auger and radiative recombination with a combined effective lifetime of 83.9 ms which leads to a minority diffusion lengt of 2.87 cm, and on the front surface, we defined a perfect electron selective contact (no surface recombination and no contact resistance) with no front reflectance. Regarding light trapping properties, we can consider perfect light trapping for photons with energy higher than bandgap, so as we can obtain the maximum potential efficiencies with the contacts proposed hereby. On the contrary, no light trapping properties can be also considered with flat surfaces whose internal reflectance values match the experimental ones reported in Fig. 4. In particular, a good general agreement can be found with an internal rear reflectance of 85% and a front internal reflectance of 36% (considering the interface between air and c-Ge with a constant refractive index of 4). The exploration of both extreme cases is justified by the 1473 K black body spectrum whose peak is at 1967 nm with most of the profitable photons with energies close to the c-Ge bandgap and, thus, low absorption coefficients. As a consequence, the light trapping properties of the device introduce a significant difference in the electrical output power (see Supplementary Information for further details about the simulated External Quantum Efficiency curves). The different performance of the explored contacts was introduced at the rear surface recombination velocity where the experimental values of Table 1 were used, in particular 588 cm/s for the case of ITO contacting the MoO_x and 156 cm/s for the case of gold. Additionally, the contact resistivity is modeled by a lumped resistance element equal to the experimental value, i.e. 55.6 mΩ cm^2 for ITO on MoO_x and 60.9 mΩ cm^2 for gold contacting the MoO_x.

In Table 2, we show the electrical performance, open circuit voltage (V_{oc}), short circuit current density (J_{sc}) and fill factor (FF), of the simulated devices with the two contacts under test for the case of no light trapping and perfect light trapping (in brackets). Additionally, we also include the case where the rear surface is directly contacted with an aluminum film where we assume no passivation ($S_{eff} = 5{\cdot}10^6$ cm/s) and no contact resistivity ($\rho_C = 0$ Ω cm^2). As we can see, both contacts with MoO_x show a much better result in V_{oc} and J_{sc} compared to the case of just aluminum due to the better rear passivation, whereas a lower FF is obtained related to the higher contact resistivity. Despite this higher parasitic resistance, the simulated electrical power demonstrates the potential benefit of the contacts proposed in this work compared to a simple aluminum rear contact. If we compare the two MoO_x contacts among them, a much better electrical result is obtained for the case of Au/MoO_x which is related to the improved selectivity of the contact that is mainly impacting on a much higher V_{oc} value. In addition, the higher V_{oc} also permits a higher FF despite similar ρ_C values for both contacts.

Regarding out-band-reflectance, we calculate for all three cases the reflected power using the experimental curves of Fig. 4 and equation (5). An out-of-band reflectance (R_{OOB}) can be also calculated by weighting the experimental data with the black body spectrum used in the simulations leading to values of 87.5% for the case of Ag/ITO/MoO_x, 83.0% for the case of just aluminum and 78.9% for Au/MoO_x. These optical properties are introduced into equation (4) to calculate the corresponding PCE. As we can see in Table 2, the contact with gold has a better PCE value of 11.7% (18.9%) compared to 11.2% (18.5%) for its counterpart with ITO, while the aluminum contact shows a very poor performance as expected. Notice that the significant difference in electric power between the explored contacts, i.e. the Au/MoO_x contact shows a factor of ~1.25 higher $P_{electric}$ than Ag/ITO/MoO_x contact, is strongly reduced when PCE is calculated due to the better exploitation of the out-of-band photons provided by Ag/ITO/MoO_x case. Although the novel contacts proposed hereby are not optimized, these simulations show that these hole selective contacts allow efficiencies at least comparable to the best efficiency (16.0%) reported in the literature for thermophotovoltaic devices based on c-Ge [12]. Further research is needed to introduce these contacts into optimized devices where their full potential can be exploited.

4. Conclusions

In this work, we report on electrical and optical characterization of hole selective contacts based on transition metal oxides for thermophotovoltaic c-Ge devices. From an electrical point of view, the best performance is obtained for MoO_x contacts compared to VO_x and WO_x. Focusing on MoO_x, this material contacted with ITO leads to a S_{eff} and ρ_C of 588 cm/s and 55.6 mΩ cm^2, respectively, and a contact selectivity parameter of 4.4. Surface passivation can be improved by the introduction of a thin (~2 nm) a-SiC_x layer, but it jeopardizes carrier transport leading to the formation of a rectifying contact. This detrimental effect can be avoided by replacing sputtered ITO by thermal evaporated gold whose higher workfunction helps in hole transport through the contact. With such metal, electrical quality of the contact improves with S_{eff} of 156 cm/s and ρ_C of 60.9 mΩ cm^2 resulting in S_{10} of 4.9. Regarding the out-of-band reflectance, higher values are obtained for the Ag/ITO/MoO_x contact compared to Au/MoO_x. Using a 1473 K black body spectrum, a best result for R_{OOB} of 87.5% is measured when ITO thickness is reduced to 20 nm. Potential system efficiencies using Ag/ITO/

Table 2
Photovoltaic figures obtained from PC-1D simulations where the rear contact is defined using the experimental S_{eff} and ρ_C values from Table 1. A rear contact fully covered with aluminum is also shown as a reference where no passivation and no contact resistance is considered. Values in brackets are referred to simulations with perfect light trapping properties. Reflected power calculated from the experimental reflectance and using equation (5). Power conversion efficiency calculated using equation (4).

	V_{oc} (mV)	J_{sc} (A·cm^{-2})	FF (%)	$P_{electrical}$ (W·cm^{-2})	$P_{reflected}$ (W·cm^{-2})	PCE (%)
Ag/ITO/MoO_x	337 (359)	0.762 (1.243)	53.6 (50.9)	0.138 (0.227)	2.671	11.2 (18.5)
Au/MoO_x	377 (390)	0.771 (1.259)	60.1 (57.4)	0.175 (0.282)	2.412	11.7 (18.9)
Al	202 (209)	0.616 (0.896)	62.8 (63.0)	0.078 (0.118)	2.541	5.7 (8.7)

MoO_x and Au/MoO_x at the rear surface of c-Ge thermophotovoltaic devices are simulated with PC-1D. Simulations show a better electrical performance of the Au/MoO_x contact, as expected from the previous characterization, while similar maximum potential system efficiencies in the range of 18–19% are obtained due to the higher reflectance for the out-of-band photons for the Ag/ITO/MoO_x contact. These results demonstrate the high potential of the contacts proposed hereby whose introduction into optimized devices will be addressed in the future.

CRediT authorship contribution statement

Isidro Martín: Writing – original draft, Validation, Methodology, Funding acquisition, Formal analysis, Conceptualization. **Gema López:** Methodology, Data curation. **Moisés Garín:** Writing – review & editing, Investigation, Funding acquisition, Data curation. **Eloi Ros:** Writing – review & editing, Validation, Investigation, Formal analysis. **Pablo Ortega:** Writing – review & editing, Validation, Methodology. **Cristóbal Voz:** Writing – review & editing, Validation, Supervision, Funding acquisition. **Joaquim Puigdollers:** Writing – review & editing, Funding acquisition.

Declaration of competing interest

The authors declare that they have no known competing financial interests or personal relationships that could have appeared to influence the work reported in this paper.

Data availability

Data will be made available on request.

Acknowledgments

This work has been supported by the Spanish government under projects PID2019-109215RB-C41 (SCALED), PID2020-116719RB-C41 (MATER ONE) and PID2020-115719RB-C21 (GETPV) funded by MCIN/AEI/10.13039/501100011033. The authors would like to thank the master student Oscar Lladós and Guillem Ayats for their help in processing the samples, Dr. Alejandro Datas from Instituto de Energía Solar (IES) in Madrid for providing the c-Ge wafers and fruitful discussions.

Appendix A. Supplementary data

Supplementary data to this article can be found online at https://doi.org/10.1016/j.solmat.2022.112156.

References

[1] T. Burger, C. Sempere, B. Roy-Layinde, A. Lenert, Present efficiencies and future opportunities in thermophotovoltaics, Joule 4 (2020) 1660–1680, https://doi.org/10.1016/j.joule.2020.06.021.
[2] A. Datas, A. Martí, Thermophotovoltaic energy in space applications: review and future potential, Sol. Energy Mater. Sol. Cells 161 (2017) 285–296, https://doi.org/10.1016/j.solmat.2016.12.007.
[3] C. Amy, H.R. Seyf, M.A. Steiner, D.J. Friedman, A. Henry, Thermal energy grid storage using multi-junction photovoltaics, Energy Environ. Sci. 12 (2019) 334–343, https://doi.org/10.1039/C8EE02341G.
[4] A. Datas, A. Ramos, A. Martí, C. del Cañizo, A. Luque, Ultra high temperature latent heat energy storage and thermophotovoltaic energy conversion, Energy 107 (2016) 542–549, https://doi.org/10.1016/j.energy.2016.04.048.
[5] A. Licht, N. Pfiester, D. DeMeo, J. Chivers, T.E. Vandervelde, A review of advances in thermophotovoltaics for power generation and waste heat harvesting, MRS Adv 4 (2019) 2271–2282, https://doi.org/10.1557/adv.2019.342.
[6] Z. Zhou, E. Sakr, Y. Sun, P. Bermel, Solar thermophotovoltaics: reshaping the solar spectrum, Nanophotonics 5 (2016) 1–21, https://doi.org/10.1515/nanoph-2016-0011.
[7] D.M. Bierman, A. Lenert, W.R. Chan, B. Bhatia, I. Celanovic, M. Soljacic, E. N. Wang, Enhanced photovoltaic energy conversion using thermally based spectral shaping, Nat. Energy 1 (2016), 16068, https://doi.org/10.1038/nenergy.2016.68.
[8] Z. Omair, G. Scranton, L.M. Pazos-Autón, T.P. Xiao, M.A. Steiner, V. Ganapati, P. F. Peterson, J. Holzrichter, H. Atwater, E. Yablonovitch, Ultraefficient thermophotovoltaic power conversion by band-edge spectral filtering, Proc. Natl. Acad. Sci. USA 116 (2019) 15356–15361, https://doi.org/10.1073/pnas.1903001116.
[9] D. Fan, T. Burger, S. McSherry, B. Lee, A. Lenert, S.R. Forrest, Near-perfect photon utilization in an air-bridge thermophotovoltaic cell, Nature 586 (2020) 237–241, https://doi.org/10.1038/s41586-020-2717-7.
[10] D.N. Woolf, E.A. Kadlec, D. Bethke, A.D. Grine, J.J. Nogan, J.G. Cederberg, D. B. Burckel, T.S. Luk, E.A. Shaner, J.M. Hensley, High-efficiency thermophotovoltaic energy conversion enabled by a metamaterial selective emitter, Optica 5 (2018) 213, https://doi.org/10.1364/OPTICA.5.000213.
[11] A. LaPotin, K.L. Schulte, M.A. Steiner, K. Buznitsky, C.C. Kelsall, D.J. Friedman, E. J. Tervo, R.M. France, M.R. Young, A. Rohskopf, S. Verma, E.N. Wang, A. Henry, Thermophotovoltaic efficiency 40, Nature 604 (2022) 287–291, https://doi.org/10.1038/s41586-022-04473-y.
[12] J. Fernández, F. Dimroth, E. Oliva, M. Hermle, A.W. Bett, Back-surface optimization of germanium TPV cells, AIP Conf. Proc. 890 (2007) 190–197, https://doi.org/10.1063/1.2711736.
[13] J. van der Heide, N.E. Posthuma, G. Flamand, W. Geens, J. Poortmans, Cost-efficient thermophotovoltaic cells based on germanium substrates, Sol. Energy Mater. Sol. Cells 93 (2009) 1810–1816, https://doi.org/10.1016/j.solmat.2009.06.017.
[14] C. Battaglia, X. Yin, M. Zheng, I.D. Sharp, T. Chen, S. McDonnell, A. Azcatl, C. Carraro, B. Ma, R. Maboudian, E.M. Wallace, A. Javey, Hole selective MoO_x contact for silicon solar cells, Nano Lett. 14 (2014) 967–971, https://doi.org/10.1021/nl404389u.
[15] J. Bullock, A. Cuevas, T. Allen, C. Battaglia, Molybdenum oxide MoO_x: a versatile hole contact for silicon solar cells, Appl. Phys. Lett. 105 (2014), 232109, https://doi.org/10.1063/1.4903467.
[16] L.G. Gerling, S. Mahato, A. Morales-Vilches, G. Masmitja, P. Ortega, C. Voz, R. Alcubilla, J. Puigdollers, Transition metal oxides as hole-selective contacts in silicon heterojunctions solar cells, Sol. Energy Mater. Sol. Cells 145 (2016) 109–115, https://doi.org/10.1016/j.solmat.2015.08.028.
[17] R.A. Vijayan, S. Essig, S. De Wolf, B.G. Ramanathan, P. Löper, C. Ballif, M. Varadharajaperumal, Hole-collection mechanism in passivating metal-oxide contacts on Si solar cells: insights from numerical simulations, IEEE J. Photovoltaics 8 (2018) 473–482, https://doi.org/10.1109/JPHOTOV.2018.2796131.
[18] A. Alcañiz, G. López, I. Martín, A. Jiménez, A. Datas, E. Calle, E. Rosa, L.G. Gerling, C. Voz, C. del Cañizo, R. Alcubilla, Germanium photovoltaic cells with MoO_x hole-selective contacts, Sol. Energy 181 (2019) 357–360, https://doi.org/10.1016/j.solener.2019.02.009.
[19] I. Martín, G. López, M. Garín, C. Voz, P. Ortega, J. Puigdollers, Effect of the thickness of amorphous silicon carbide interlayer on the passivation of c-Ge surface by aluminum oxide films, Surface. Interfac. 31 (2022), 102070, https://doi.org/10.1016/j.surfin.2022.102070.
[20] R.A. Sinton, A. Cuevas, Contactless determination of current–voltage characteristics and minority-carrier lifetimes in semiconductors from quasi-steady-state photoconductance data, Appl. Phys. Lett. 69 (1996) 2510–2512, https://doi.org/10.1063/1.117723.
[21] I. Martín, A. Alcañiz, A. Jiménez, G. López, C. del Cañizo, A. Datas, Application of quasi-steady-state photoconductance technique to lifetime measurements on crystalline germanium substrates, IEEE J. Photovoltaics 10 (2020) 1068–1075, https://doi.org/10.1109/JPHOTOV.2020.2981839.
[22] S. Guo, G. Gregory, A. Gabor, W. Schoenfeld, K.O. Davis, Detailed investigation of TLM contact resistance measurements on crystalline silicon solar cells, Sol. Energy 151 (2017) 163–172, https://doi.org/10.1016/j.solener.2017.05.015.
[23] R. Brendel, R. Peibst, Contact selectivity and efficiency in crystalline silicon photovoltaics, IEEE J. Photovoltaics 6 (2016) 1413–1420, https://doi.org/10.1109/JPHOTOV.2016.2598267.
[24] T. Zhang, C.-Y. Lee, Y. Wan, S. Lim, B. Hoex, Investigation of the thermal stability of MoO_x as hole-selective contacts for Si solar cells, J. Appl. Phys. 124 (2018), 073106, https://doi.org/10.1063/1.5041774.
[25] Z. Wang, P. Li, Z. Liu, J. Fan, X. Qian, J. He, S. Peng, D. He, M. Li, P. Gao, Hole selective materials and device structures of heterojunction solar cells: recent assessment and future trends, Apl. Mater. 7 (2019), 110701, https://doi.org/10.1063/1.5121327.
[26] Y. Park, V. Choong, Y. Gao, B.R. Hsieh, C.W. Tang, Work function of indium tin oxide transparent conductor measured by photoelectron spectroscopy, Appl. Phys. Lett. 68 (1996) 2699–2701, https://doi.org/10.1063/1.116313.
[27] K. Sugiyama, H. Ishii, Y. Ouchi, K. Seki, Dependence of indium–tin–oxide work function on surface cleaning method as studied by ultraviolet and x-ray photoemission spectroscopies, J. Appl. Phys. 87 (2000) 295–298, https://doi.org/10.1063/1.371859.
[28] R. Schlaf, H. Murata, Z.H. Kafafi, Work function measurements on indium tin oxide films, J. Electron. Spectrosc. Relat. Phenom. 120 (2001) 149–154, https://doi.org/10.1016/S0368-2048(01)00310-3.
[29] D.A. Clugston, P.A. Basore, PC1D Version 5: 32-bit Solar Cell Modeling on Personal Computers, Proceedings of the 26th IEEE Photovoltaic Specialists Conference PVSC, 1997, pp. 207–210, https://doi.org/10.1109/PVSC.1997.654065.